Journal of Sound and Vibration (2001) **245**(3), 545–557
doi:10.1006/jsvi.2001.3571, available online at http://www.idealibrary.com on IDEAL®

A NUMERICAL AND EXPERIMENTAL INVESTIGATION OF THE DISSIPATION MECHANISMS OF RESONANT ACOUSTIC LINERS

C. K. W. Tam and K. A. Kurbatskii

Florida State University, Tallahassee, FL 32306-4510, *U.S.A.*

and

K. K. Ahuja and R. J. Gaeta, Jr.

Georgia Institute of Technology, GTRI/ATASL, Atlanta, GA 30332-0844, *U.S.A.*

(*Received* 23 *October* 2000, *and in final form* 22 *January* 2001)

In a recent investigation, it was found by direct numerical simulation that sound waves at high intensity can induce vortex shedding at the mouths of the resonators of an acoustic liner. Measurements from their numerical simulations indicate that the rate at which kinetic energy is transferred to the shed vortices can be much higher than the viscous dissipation rate. Thus vortex shedding is a dominant dissipation mechanism of resonant acoustic liners. This paper reports the results of a co-ordinated investigation aiming at validating the observations and measurements of direct numerical simulation experimentally. The experiment uses a normal incidence impedance tube. Good agreements are found between the measured absorption coefficients of the physical experiment and direct numerical simulation over a broad range of frequencies and sound pressure levels. A separate visualization experiment confirms the observation of shed vortices at high incident sound intensity.

1. INTRODUCTION

Acoustic liners are invariably installed in present day jet engines for noise suppression purpose. They are found to be effective in suppressing fan noise to an acceptable level. Although acoustic liners have been widely used since the 1970s, the actual mechanisms by which sound is dissipated remains an open question. In the case of resonant liners, most of the dissipation takes place around the openings of the resonators. The typical size of the openings is less than 1 mm in diameter. Due to the smallness of the openings, no experimental measurements of the flow in and around such a resonator have ever been performed. (Note: Ingard and coworkers [1, 2] have conducted flow visualization studies and hot wire measurements on larger size orifices.) In the literature, a number of semi-empirical models, references [3–5] have been developed to describe the flow field and to provide an impedance value for the liner. Most of the basic ideas of these models can be traced back to a paper by Melling [6]. Melling suggested that if the sound intensity was low, the principal dissipation mechanism was wall friction around the resonator opening. If the sound intensity was high, an oscillatory turbulent jet with phase correlated to the incident sound waves developed right at the entrance of the resonator. Presumably, the conversion of sound energy to turbulence was the main mechanism of dissipation in this case. The basis of invoking the presence of a turbulent jet was the earlier experimental observations of

0022-460X/01/330545 + 13 $35.00/0

Ingard and Labate [1] and Ingard and Ising [2]. However, in the experiments, a relatively large orifice was used. Due to the large opening used in the experiment, the viscous effects could be significantly different. It is, therefore, not clear whether the oscillatory turbulent jet model of reference [7] is applicable to present day resonant liners.

Recently, Tam and Kurbatskii [8] investigated the dissipation mechanisms of a slit resonator by direct numerical simulation. One main advantage of direct numerical simulation is that the smallness of the resonator is not a hindrance. Further, the exact viscous effect can easily be imposed on the simulation. By using a properly designed mesh, all the essential physics involved can be incorporated in the numerical model and computation.

Tam and Kurbatskii found that at low incident sound intensity, dissipation was caused primarily by a jet-like oscillatory laminar boundary layer formed close to the walls of the resonator opening. The rate of energy dissipation by viscosity associated with the velocity gradients of the jet-like flow is relatively low. The simulation was repeated using increasing incident sound levels. The formation of a turbulent jet was not found even for sound pressure levels as high as 156 dB. Instead, vortex shedding at the mouth of the resonator was observed at moderate to high incident sound intensity. The shed vortices carried off significant amount of kinetic energy. The kinetic energy, once imparted to the vortices, could not be reverted back to acoustic energy. It is eventually dissipated by molecular viscosity. When vortex shedding occurs, there is a significant increase in energy dissipation rate. This is most desirable from the acoustic liner standpoint.

Vortex shedding as a flow phenomenon is not new. It has been found to occur in many types of flow of engineering significance. However, the observation of vortex shedding at the mouths of the resonators of a resonant liner with openings of 1 mm or less has not been reported in the literature. To ensure that this is not an artifact of numerical simulation, a co-ordinated investigation between numerical simulation and physical experiment is most desirable. The objective of the present investigation is to perform a numerical simulation and a corresponding physical experiment independently to validate the computationally observed vortex-shedding phenomenon. Furthermore, the computed dissipation rate and the experimentally measured dissipation rate over a range of incident sound frequencies and intensities are to be compared. This provides a quantitative confirmation of the reliability of numerical simulation results. This paper reports the results of the investigation.

Details of the comparisons between numerical simulations and physical experiment are given in section 4 of this paper. It will be reported that the measured absorption coefficients from numerical simulation are found to agree well with normal incidence impedance tube experimental measurements over an extended range of frequencies and sound intensities. A separate visualization experiment confirms the observation of shed vortices.

2. NUMERICAL SIMULATION

A series of numerical simulations of the flow and acoustic fields of a slit resonator driven by incident plane acoustic waves is carried out. The objective is to compare the dissipation rate of the numerical simulation with that measured in a normal incidence impedance tube experiment. The experiment is described in the next section. The computation algorithm used is similar to that of reference [8]. The dimensions of the resonator are taken to be nearly identical to that of the physical experiment. Figure 1 shows the computation domain. Plane acoustic waves created by the boundary condition on the top boundary of the computation domain are incident normally on the resonator and the adjacent wall. Here, normal incidence is chosen to simulate the condition inside a normal incidence impedance tube of the companion experiment.

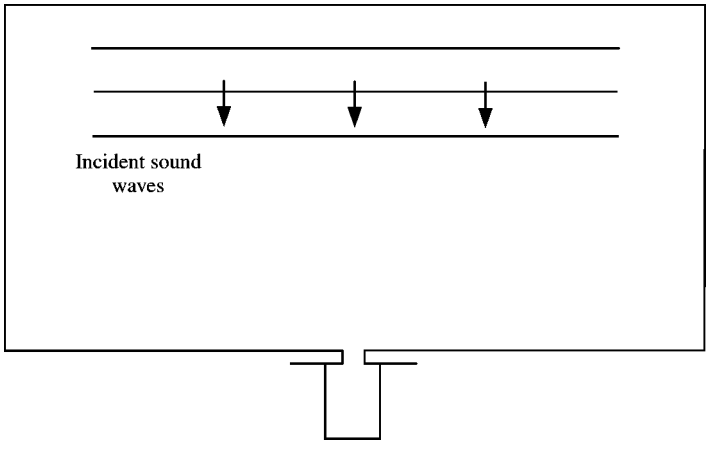

Figure 1. The computation domain.

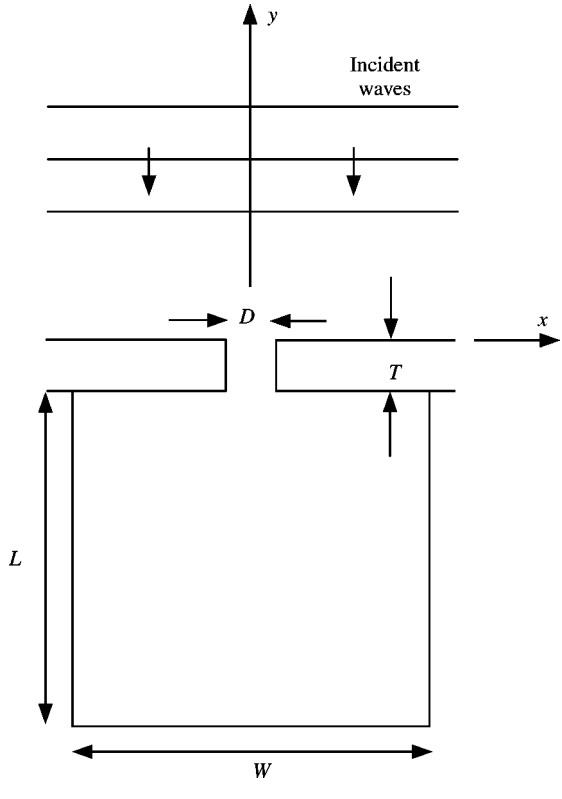

Figure 2. The slit resonator model used in the numerical simulation.

Figure 2 shows the slit resonator used in the present study. The dimensions are $D = T = 0{\cdot}8$ mm, $L = 36D$, $W = 28D$. Figure 3 shows the mesh size distribution and the different subdomains inside the resonator used in the computation. The subdomain at the resonator opening has the smallest mesh size. A square mesh is used with $\Delta x = \Delta y = D/80$, where D is the width of the opening. This mesh size is found to be able to resolve Stokes'

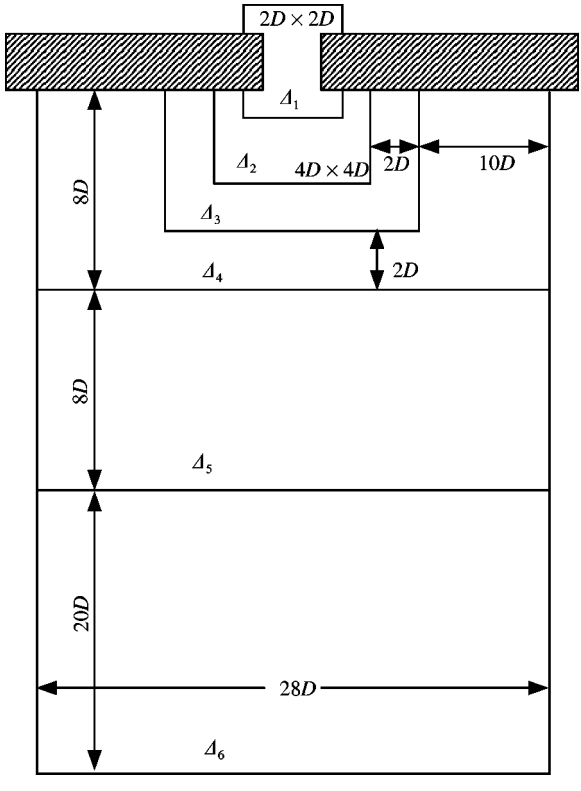

Figure 3. Grid distribution and subdomains inside and at the mouth of the slit resonator. Mesh size: $\Delta_1 = 0{\cdot}0125D$, $\Delta_n = 2^{n-1}\Delta_1$, $n = 2, \ldots, 6$.

viscous layer adjacent to the wall surfaces for frequencies up to 10 kHz. The mesh size of adjacent subdomain increases by a factor of 2 in the direction going away from the opening of the resonator. Outside the resonator, there are eight layers of mesh; again the adjacent mesh size increases by a factor of 2. The mesh size distribution and the size of the different subdomains are the same as in reference [8].

The governing equations are the compressible Navier–Stokes equations. In dimensionless form with D (the width of the resonator opening) as the length scale, a_∞ (the speed of sound) as the velocity scale, D/a_∞ as the time scale, ρ_∞ (ambient gas density) as the density scale, $\rho_\infty a_\infty^2$ as the pressure and stress scale, these equations may be written in the form

$$\frac{\partial \rho}{\partial t} + \frac{\partial \rho u_j}{\partial x_j} = 0, \tag{1}$$

$$\frac{\partial u_i}{\partial t} + u_j \frac{\partial u_i}{\partial x_j} = -\frac{1}{\rho}\frac{\partial p}{\partial x_i} + \frac{\partial \tau_{ij}}{\partial x_j}, \tag{2}$$

$$\frac{\partial p}{\partial t} + u_j \frac{\partial p}{\partial x_j} + \gamma p \frac{\partial u_j}{\partial x_j} = 0, \tag{3}$$

where $\tau_{ij} = (1/R_D)(\partial u_i/\partial x_j + \partial u_j/\partial x_i)$ and $R_D = Da_\infty/v$ is the Reynolds number. In the energy equation (3), viscous dissipation and thermal conduction are neglected. They are unimportant for the present physical problem.

The Navier–Stokes equations are discretized according to the Dispersion–Relation–Preserving (DRP) scheme (see references [9, 10]). A seven-point symmetric stencil is used in each subdomain. Outside the five subdomains with the smallest mesh, the viscous effect is unimportant. Thus, instead of the Navier–Stokes equation, the Euler equations are solved (obtained by setting $\tau_{ij} = 0$ in equation (2)). At the subdomain interface, special stencils both in space and time are used. The method to construct these stencils is discussed in the appendix of reference [8]. Effectively, the multiple-size-mesh multiple-time-step DRP scheme is used as the computation algorithm. In addition, to eliminate spurious short numerical waves and to promote numerical stability, artificial selective damping, see reference [11], is added to the computation algorithm. The same distribution of the artificial mesh Reynolds number used in reference [8] is employed in the present work. The DRP scheme is a time accurate marching scheme. In all the numerical simulations performed in the present investigation, the numerical solutions are marched to a time periodic state before measurements are made.

Following reference [8], the split variable method (see reference [12]) is adopted to implement the boundary conditions at the outside boundary of the computation domain. As discussed in reference [8], the boundary conditions perform two functions. First, they must generate the incident and the reflected sound waves in the absence of the resonator (see Figure 1). When the resonator is added to the wall, additional acoustic disturbances are generated. The boundary condition must allow these acoustic disturbances to exit the computation domain with little reflection. The exact incident and reflected plane acoustic wave system is given in reference [8]. In the split variable method, the flow variables are divided into two parts. One part is the incident and reflected wave system mentioned above. The other part is the disturbances generated by the presence of the resonator. A perfectly matched layer (PML) (see reference [13]) is added just outside the computation domain. The flow variables computed in the PML are the acoustic disturbances generated by the resonator. They are obtained by subtracting the incident and reflected acoustic wave system from the total field variables of the computation. The PML automatically absorbs all the outgoing acoustic disturbances with minimal reflection.

In the companion normal incidence impedance tube experiment (see section 3) it is found that the incident waves may contain a number of harmonics. Figure 4 shows a typical incident wave spectrum. In this case, the incident sound has a frequency of 1 kHz at 150 dB nominal. The spectrum is dominated by the fundamental. The harmonics are more than 22 dB, less in intensity. For this type of incident sound wave spectrum, only the fundamental is included in the simulation. That is, the normal incident sound waves consist of a single tone. However, it has been measured in the normal incidence impedance tube experiment that the harmonics in a few special cases are exceptionally strong. Figure 5 shows the case of incident sound at 2 kHz frequency and 150 dB nominal. The first and second harmonics are just a few dB lower in intensity than the fundamental. In these special cases, a three-wave-system with amplitudes given by experimental measurements is used as incident waves. In this way, each numerical simulation matches the experimental conditions of the corresponding normal incidence impedance tube experiment.

Figure 6 shows the computed density field around the mouth of the resonator for the case of an incident wave at 1 kHz and 130 dB in intensity. This figure clearly shows that vortex shedding is induced by the incident sound waves. Whenever vortex shedding occurs, the energy dissipation rate increases dramatically. With vortex shedding, acoustic energy is

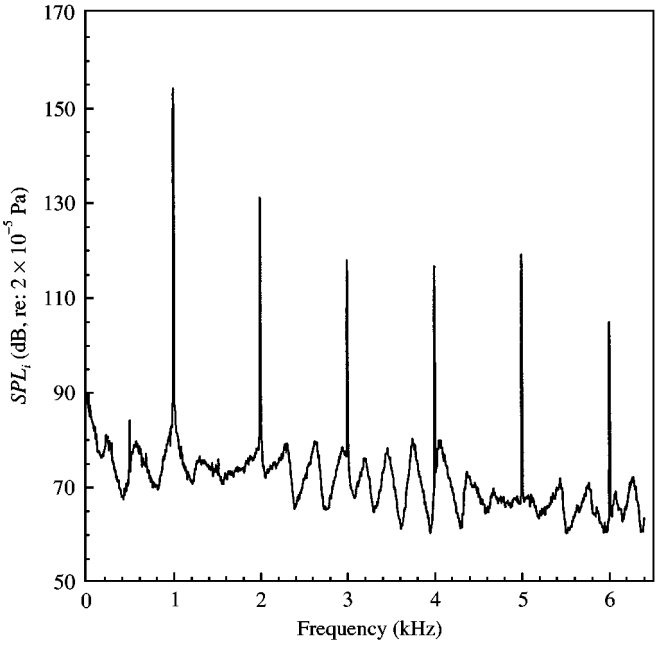

Figure 4. Measured incident sound pressure spectrum for the case of $f = 1$ kHz and 150 dB nominal SPL; $\Delta f = 4$ Hz.

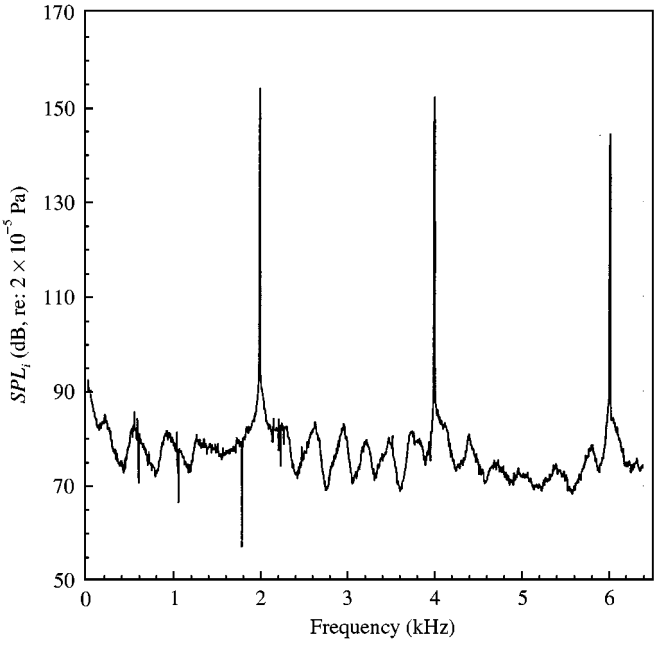

Figure 5. Measured incident sound pressure spectrum for the case of $f = 2$ kHz and 150 dB nominal SPL; $\Delta f = 4$ Hz.

dissipated in two ways; by viscous dissipation and by the transfer of acoustic energy to the kinetic energy of the vortices. The kinetic energy of the vortices is subsequently dissipated by viscosity.

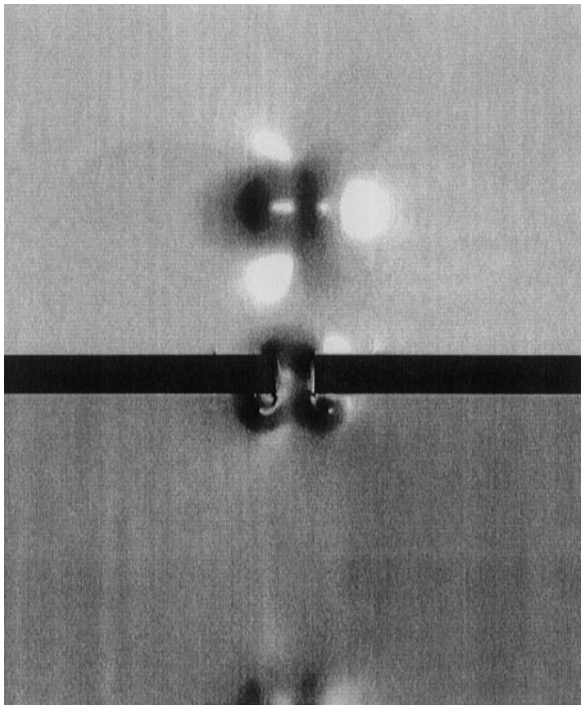

Figure 6. Density field near the mouth of the slit resonator showing the shedding of vortices. $f = 1$ kHz, SPL = 130 dB.

To compare the energy dissipation rate of the numerical simulation with experiment, both the viscous dissipation and the rate at which energy is transferred to the shed vortices are computed from the numerical output. The time averaged viscous dissipation rate, $\bar{D}(x, y)$, at a point (x, y) is given by

$$\bar{D}(x, y) = \frac{1}{T} \int_0^T \tau_{ij} \frac{\partial u_i}{\partial x_j} \mathrm{d}t, \tag{4}$$

where T is the period of the incidence sound. The total energy dissipation rate due to molecular viscosity for the entire resonator is

$$E_{viscous} = \iint_{resonator} \bar{D}(x, y)\, \mathrm{d}x\, \mathrm{d}y. \tag{5}$$

Let V_θ be the rotational velocity of a vortex. The kinetic energy of the vortex per unit span, K, is equal to

$$K = \pi \int_0^R \rho(r) V_\theta^2(r) r\, \mathrm{d}r, \tag{6}$$

where r is the radial distance measured from the center of the vortex and R is the size of the vortex. By counting the number of vortices shed over a long period of time, the number of

vortices shed per period of oscillation, N, is measured. The rate at which energy is transferred to the shed vortices, $E_{shedding}$, may now be found by

$$E_{shedding} = \frac{\langle K \rangle N}{T}, \tag{7}$$

where $\langle\ \rangle$ is the ensemble average.

By combining (5) and (7), the total energy dissipation rate due to both mechanisms is

$$E_{dissipation} = E_{viscous} + E_{shedding}\,. \tag{8}$$

As a measure of the efficiency of the resonant liner, it is noted that the energy flux of the incident acoustic waves through an area equal to the opening of the slit resonator is equal to (per unit length of the slit)

$$E_{incident} = \frac{\overline{p^2} D}{\rho_\infty a_\infty}, \tag{9}$$

where p is the pressure of the incident sound waves and the overbar indicates the time average. Of importance is the ratio $E_{dissipation}/E_{incident}$. This quantity is measured for each numerical simulation to be used for comparison with the dissipation measurements of the normal incidence impedance tube experiment (see section 4).

3. NORMAL INCIDENCE IMPEDANCE TUBE EXPERIMENT

Normal incidence impedance tube experiments were conducted to validate the results of the numerical simulations. The impedance tube had a circular cross-section with an inner diameter of 2·85 cm. The general specification of the impedance tube is detailed in reference [14]. An orifice plate with a 0·8 mm wide slit-orifice was placed at the end of the tube backed by a cavity of 2·88 cm depth. Thus the slit width, cavity depth and slit area to cavity

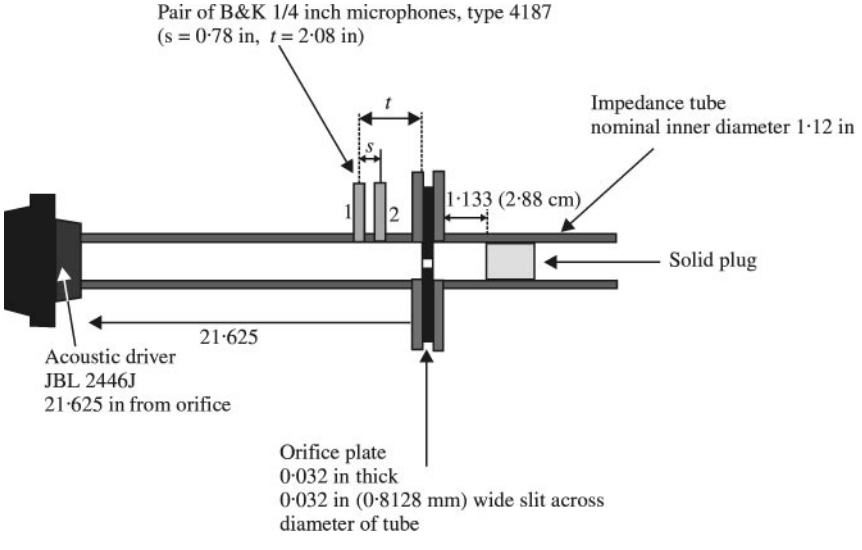

Figure 7. Experimental setup of GTRI impedance tube with slit-orifice cavity. All dimensions are in inches.

area ratio are almost identical between the experiment and the computation model (see section 2). A high intensity acoustic driver mounted at the other end of the impedance tube was used to produce the incident acoustic waves. A sinusoidal input from a function generator was supplied to a JBL acoustic driver via a Carvin Amplifier. The incident and reflected acoustic waves inside the tube were measured by the Two Microphone Method originally described by Chung and Blaser [15]. The two microphones were flush mounted on the wall of the impedance tube. The location of the microphones and the entire experimental setup are shown schematically in Figure 7. The test conditions are given in Table 1.

The cross-spectra data from the two microphones were processed with an HP 3667A Signal Analyzer. The data were then fed to a Pentium II platform to be used in the Chung and Blaser algorithm for the Two Microphone Method. The amplitude of the discrete tone was fixed at the nominal incident sound pressure level prescribed in Table 1. Data from the microphones were analyzed from 0 to 6400 Hz with a bandwidth of 4 Hz and 64 averages. Typical incident sound spectra are shown in Figures 4 and 5.

In addition to the acoustic experiment using the normal incidence impedance tube, a separate visualization experiment was performed using an acrylic tube of nominally the same dimensions as the steel impedance tube shown in Figure 7. A state-of-the-art TSI

TABLE 1
Test conditions

Frequency kHz	Nominal incident sound pressure levels dB
1·0	130, 150
2·0	130, 150
3·0	130, 150
4·0	130, 150
6·0	130, 150

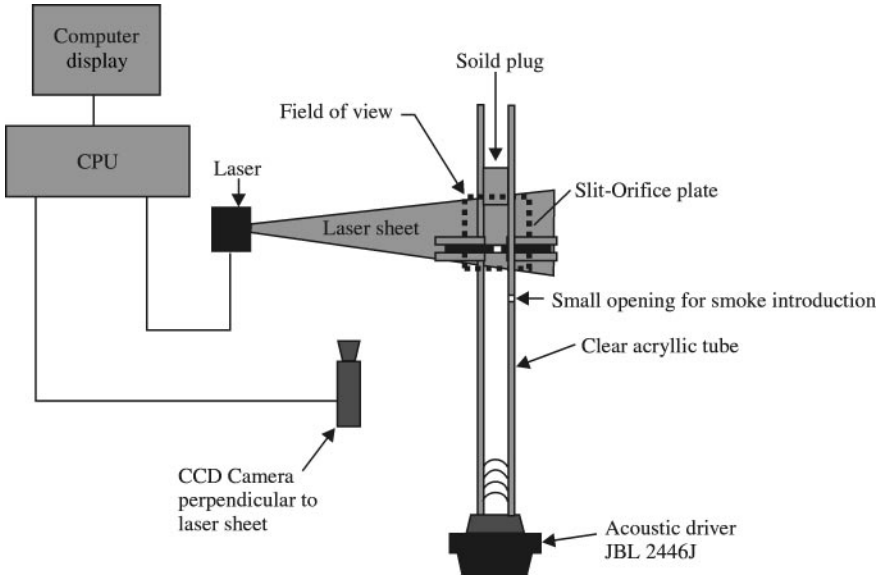

Figure 8. Experimental setup of acoustic flow visualization apparatus.

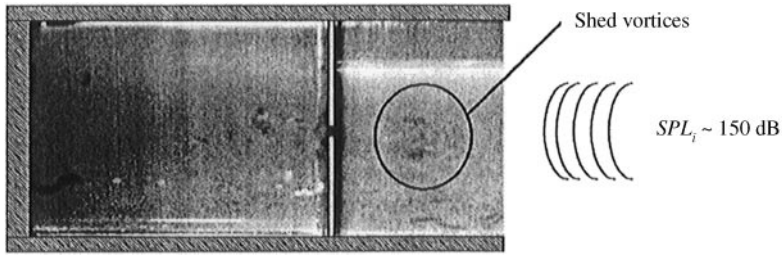

Figure 9. Flow visualization showing shed vortices near slit-orifice. Sound frequency = 1000 Hz. Sound pressure level 150 dB nominal.

TABLE 2
Measured incident sound pressure level (SPL)

Frequency kHz	130 dB nominal dB	150 dB nominal dB
1·0	132·73	156·08
2·0	135·22	*
3·0	137·92	156·36
4·0	139·52	157·97
6·0	137·44	155·73

* Two harmonics are included
2 kHz, SPL = 155·65 dB
4 kHz, SPL = 153·81 dB
6 kHz, SPL = 146·11 dB

power view particle image velocimeter (PIV) system was used to introduce a laser sheet across the width of the slit-orifice and cavity. The laser sheet illuminated incense smoke that was allowed to fill the tube before the acoustic driver was turned on. For optical observation, the system used a high resolution 30 frames per second CCD camera, dual-YAG lasers and a Laser Pulse Light Arm for the delivery of the laser beam. A schematic diagram of the entire visualization experiment apparatus is given in Figure 8. The objective of the flow visualization experiment is to obtain images to allow visualization of the instantaneous fluid motion. Of special interest is the visualization of shed vortices near the opening of the slit-orifice.

Figure 9 shows a flow visualization picture obtained at 1 kHz incident sound waves and 150 dB nominal intensity. This picture is quite typical of the set of pictures obtained in the experiment. As can be seen, there are shed vortices near the slit-orifice. Figure 9 and similar images provide clear evidence of the presence of shed vortices induced by incidence sound waves. They confirm the original observation of reference [8] using direct numerical simulation.

4. COMPARISONS BETWEEN MEASURED RESULTS FROM NUMERICAL SIMULATION AND NORMAL INCIDENCE IMPEDANCE TUBE EXPERIMENT

In order to be able to make direct comparisons between experimental measurements and those from direct numerical simulation, the normal incidence impedance tube experiment was performed first. The measured incident sound intensity and that of the harmonics (if the amplitudes are high enough) are then used in the numerical simulation. The measured incident sound intensities at different frequencies are tabulated in Table 2.

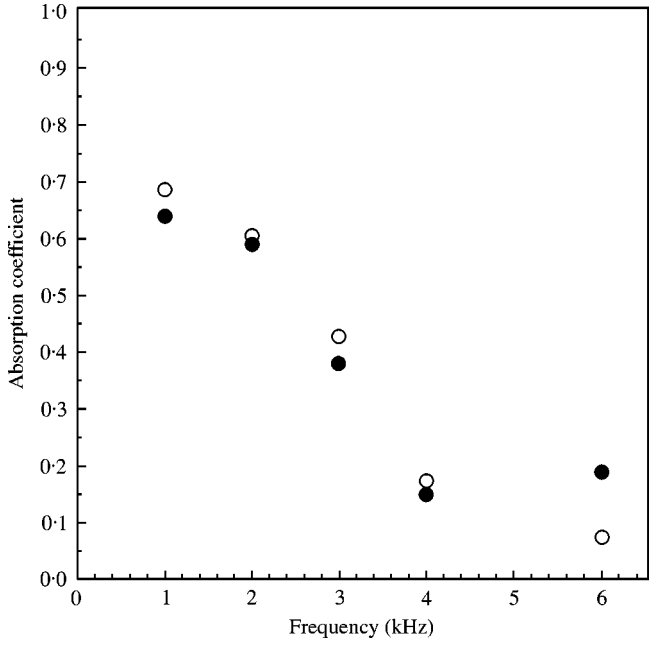

Figure 10. Comparison between the absorption coefficients measured by the normal incidence impedance tube experiment, ●, and those from direct numerical simulation, ○. Nominal incident sound pressure level = 150 dB.

The numerical simulation provides the ratio $E_{dissipation}/E_{incident}$. It is necessary to convert this ratio into an absorption coefficient corresponding to the normal incidence impedance tube experimental configuration. Let σ_s be the area of the slit and σ_t be the cross-sectional area of the impedance tube. Suppose the energy flux of the incident sound is $\overline{p_i^2}/\rho_\infty a_\infty$ then the total incident energy flux is equal to $(\overline{p_i^2}/\rho_\infty a_\infty)\sigma_t$. The energy flux incident on the slit is equal to $\overline{p_i^2}\sigma_s/\rho_\infty a_\infty$. The rate at which energy is dissipated or absorbed by the slit according to the numerical simulation is equal to $(E_{dissipation}/E_{incident})$ $(\overline{p_i^2}/\rho_\infty a_\infty)\sigma_s$. Hence the absorption coefficient (fraction of total sound power absorbed) is given by

$$\begin{aligned}\text{Absorption coefficient} &= \frac{(E_{dissipation}/E_{incident})/(\overline{p_i^2}/\rho_\infty a_\infty)\sigma_s}{(\overline{p_i^2}/\rho_\infty a_\infty)\sigma_t} \\ &= (E_{dissipation}/E_{incident})\,(\sigma_s/\sigma_t).\end{aligned} \tag{10}$$

Figure 10 shows a comparison of the absorption coefficients measured experimentally and those measured from direct numerical simulation at a nominal incident sound intensity of 150 dB. In this work, numerical computations were conducted over a sufficient number of cycles to ensure that dynamic steady state was achieved before measurements were made. As it is evident, the agreement is excellent for all the low frequency cases. There is some noticeable difference at 6 kHz. This could be the result of measurement error. At frequencies sufficiently above the resonator tuned frequency, resonator impedance becomes dominated by orifice inertia reactance and hence $R \ll |X|$. At these frequencies, it becomes difficult to accurately measure R and the absorption coefficient in an impedance tube. Also, the present numerical algorithm was designed specifically for accurate simulation of waves with frequency up to 6 kHz. Figure 11 shows a similar comparison at nominal incident sound

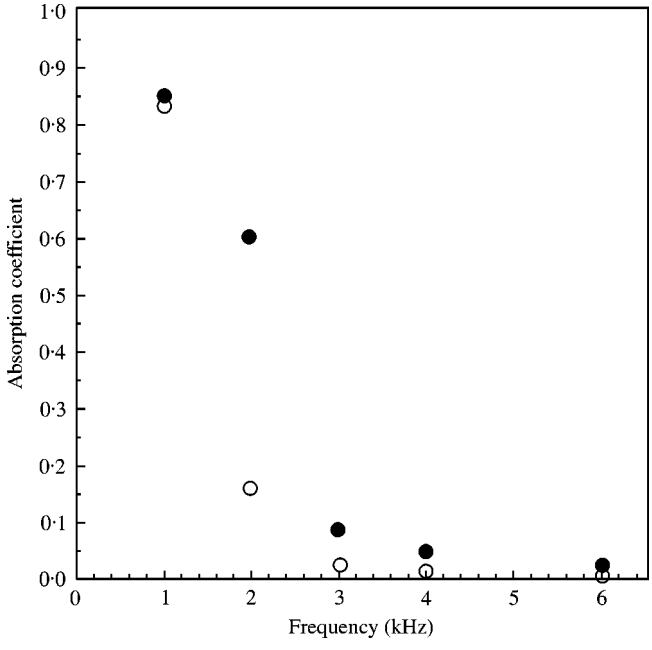

Figure 11. Comparison between the absorption coefficients measured by the normal incidence impedance tube experiment, ●, and those from direct numerical simulation, ○. Nominal incident sound pressure level = 130 dB.

intensity of 130 dB. There are good agreements at all frequencies except 2 kHz. At present, there is no definitive explanation of the large discrepancy. A plausible reason has, however, been suggested as follows. It is noted that the absorption coefficient has a very steep gradient between 1 and 3 kHz. At 1 kHz, there is vortex shedding in the numerical simulation but no vortex shedding at 3 kHz. It is speculated that the experiment may differ slightly from the numerical simulation. Due to the slight difference, there may be vortex shedding in the experiment and no vortex shedding in the simulation. This results in a large absorption coefficient for the experiment. The suggestion appears to be probable, but not easy to confirm.

It is interesting to point out that vortex shedding was observed in the numerical simulation when the incident sound pressure level is nominally at 150 dB. However, at 130 dB nominal sound pressure level, only the 1 kHz case has vortex shedding; apparently the system resonance frequency is 1 kHz. Figures 10 and 11 indicate that the absorption coefficient is small whenever vortex shedding is not observed. This is a direct confirmation that vortex shedding is a powerful sound dissipation mechanism for resonant liners.

5. CONCLUSION

A co-ordinated numerical and experimental investigation of the dissipation mechanisms of slit resonator with dimensions typical of those of present day resonant acoustic liners has been carried out. In a previous work, Tam and Kurbatskii [8], using direct numerical simulation, observed the occurrence of vortex shedding at the mouth of the resonator. Their numerical results indicate that vortex shedding is an important acoustic energy dissipation mechanism. Present flow visualization experiment confirms the presence of shed vortices near the mouth of the slit in direct support of the occurrence of vortex shedding. Acoustic

absorption coefficients calculated from numerical simulation are in good agreement with normal incidence impedance tube measurements over a wide range of frequencies and incident sound pressure levels. The good agreement provides strong support for the validity of the observations and measurements of direct numerical simulation. It is hoped that there is now sufficient confidence in the use of numerical simulation to explore the flow physics of acoustic liners further. It is worthwhile to point out that the results obtained have been derived without recourse to concepts of mass reactance as used in standard liner technology literature and represent a radical departure from conventional thinking. However, the present work must be regarded as an initial effort in clarifying the macroscopic description of acoustic liner properties in terms of impedance. Further studies are obviously needed to provide a firmer physical basis for such concepts.

ACKNOWLEDGMENTS

This work was supported by NASA Grant NAG 1-1986 to the Florida State University and NAG 1-1734 to the Georgia Tech Research Institute. The authors wish to thank Mr. Tony Parrott, Mr. Mike Jones and Dr. Willie Watson of the NASA Langley Research Center for their support of this work and for their technical comments and suggestions.

REFERENCES

1. U. INGARD and S. LABATE 1950 *Journal of the Acoustical Society of America* **22**, 211–219. Acoustic circulation effects and the nonlinear impedance of orifices.
2. U. INGARD and H. ISING 1967 *Journal of the Acoustical Society of America* **42**, 6–17. Acoustic nonlinearity of an orifice.
3. A. S. HERSH and B. E. WALKER 1995 *American Institute of Aeronautics and Astronautics Paper 95-0078*. Acoustic behavior of Helmholtz resonators: Part 1, Nonlinear model.
4. R. E. KRAFT, J. YU and H. W. KWAN 1997 *American Institute of Aeronautics and Astronautics Paper 97-1653*. Acoustic treatment impedance models for high frequencies.
5. M. JONES 1997 *American Institute of Aeronautics and Astronautics Paper 97-1649*. An improved model for parallel-element liner impedance prediction.
6. T. H. MELLING 1973 *Journal of Sound and Vibration* **29**, 1–65. The acoustic impedance of perforates at medium and high sound pressure levels.
7. B. T. ZINN 1970 *Journal of Sound and Vibration* **13**, 347–356. A theoretical study of non-linear damping by Helmholtz resonators.
8. C. K. W. TAM and K. A. KURBATSKII 2000 *American Institute of Aeronautics and Astronautics Journal* **38**, 1331–1339. Micro-fluid dynamics and acoustics of resonant liners.
9. C. K. W. TAM and J. C. WEBB 1993 *Journal of Computational Physics* **107**, 262–281. Dispersion-relation-preserving finite difference schemes for computational acoustics.
10. C. K. W. TAM 1995 *American Institute of Aeronautics and Astronautics Journal* **33**, 1788–1796. Computational aeroacoustics: issues and methods.
11. C. K. W. TAM, J. C. WEBB and Z. DONG 1993 *Journal of Computational Acoustics* **1**, 1–30. A study of the short wave components in computation acoustics.
12. C. K. W. TAM 1998 *Journal of Computational Acoustics* **6**, 377–402. Advances in numerical boundary conditions for computational aeroacoustics.
13. C. K. W. TAM, L. AURIAULT and F. CAMBULI 1998 *Journal of Computational Physics* **144**, 213–234. Perfectly matched layer as an absorbing boundary condition for the linearized Euler equations in open and ducted domains.
14. R. J. GAETA 1988 *Ph.D. Thesis, School of Aerospace Engineering, Georgia Institute of Technology*. Liner Impedance Modification by Varying Perforate Orifice Geometry.
15. J. Y. CHUNG and D. A. BLASER 1980 *Journal of the Acoustical Society of America* **68**, 907–921. Transfer function method of measuring In-duct acoustic properties: I. theory.